

論文の内容の要旨

論文題目

Effects of inter-ligand interactions on the redox and optical properties of thiolate-protected gold superatoms

(チオラート保護金超原子の酸化還元挙動と光学特性
に対する配位子間相互作用の効果)

氏名 重田 翼

1. Introduction

Gold clusters composed of several to hundreds of gold atoms can be viewed as superatoms because they take atom-like electron configuration by accommodating valence electrons in quantized orbitals labeled as 1S, 1P, 1D, 2S,... [1]. In order to utilize the Au superatoms as novel materials and building units of functional devices [2], their surface must be passivated with organic ligands such as phosphines, thiolates (RS), alkynyls, and *N*-heterocyclic carbenes. Recent examples have illustrated that the ligands do not just protect the Au superatoms, but also directly affect their structures, reactivity, and physicochemical properties. For example, chiral ligands induce circular dichroism in the optical transition within the Au superatoms [3] and non-covalent interactions between the ligands such as CH- π and/or π - π interactions enhances the robustness and photoluminescence (PL) quantum yields of the Au superatoms [4, 5]. These findings suggest a possibility that the geometric structures and associated optical and redox properties of Au superatoms are tuned by controlling the effects of the interactions between protecting ligands. In my doctoral study, I studied how the structures of the ligand tail groups affect the structures and properties of Au superatoms. To this end, I herein used two types of thiol ligands; *N*-(2-mercaptopropionyl)glycine (PGSH, Figure 1a) and cyclohexanethiol (cHexSH, Figure 1b) with a secondary α -carbon

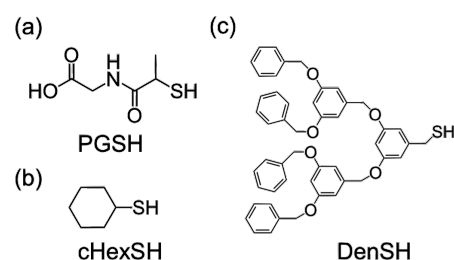


Figure 1 Structures of (a) PGSH, (b) cHexSH, and (c) DenSH. The generation of DenSH is two.

and the Fréchet-type dendritic thiols (DenSH, Figure 1c) [6] with the first and second generation (Den^{G1}SH, Den^{G2}SH) having benzyloxy groups. The target superatom is $[\text{Au}_{25}(\text{SR})_{18}]^z$ in which six units of $\text{Au}_2(\text{SEtPh})_3$ fully cap an icosahedral (Ih) Au_{13} core with a closed electron configuration of $(1\text{S})^2(1\text{P})^6$ for $z = -1$ (Figure 2a) [7-9]. I synthesized $[\text{Au}_{25}(\text{SPG})_{18}]^-$ and $[\text{Au}_{25}(\text{ScHex})_{18}]^0$ and investigated how their optical absorption and reduction behavior are changed by the ligands. On the other hand, DenSH was partially introduced through ligand-exchange reaction. In addition to conventional $[\text{Au}_{25}(\text{SR})_{18}]^-$, $[\text{Au}_{23}(\text{SR})_{16}]^-$ with an anisotropic Au_{13} core was used as a precursor superatom (Figure 2b) [10]. I studied how photoluminescence (PL) properties of $[\text{Au}_{25}(\text{SR})_{18}]^-$ and $[\text{Au}_{23}(\text{SR})_{16}]^-$ were changed dependent on the number and generation of DenS ligands.

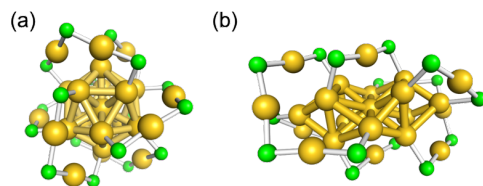


Figure 2 Crystal structures of (a) $[\text{Au}_{25}(\text{SR})_{18}]^-$ [7, 8] and (b) $[\text{Au}_{23}(\text{SR})_{16}]^-$ [10]. R group is omitted for clarity.

2. HOMO-LUMO gap widening in $[\text{Au}_{25}(\text{SR})_{18}]^-$ protected by *N*-(2-mercaptopropionyl)glycine

$[\text{Au}_{25}(\text{SPG})_{18}]^-$ was synthesized and identified as follows: $\text{Au}_{25}(\text{SPG})_{18}$ cluster was fractionated by polyacrylamide gel electrophoresis from crude Au:SPG cluster prepared according to the previous report with modification [11]. From the isotope pattern analysis of the electrospray ionization (ESI)-mass spectrum, the total charge of $\text{Au}_{25}(\text{SPG})_{18}$ was determined to be -1 .

The profiles of optical absorption spectrum and extended X-ray absorption fine structure (EXAFS) oscillation of $[\text{Au}_{25}(\text{SPG})_{18}]^-$ are significantly different from those of conventional $[\text{Au}_{25}(\text{SEtPh})_{18}]^-$ (PhEtSH = 2-phenylethanethiol), but is similar to those of $[\text{Au}_{23}(\text{ScHex})_{16}]^-$ (Figure 3), suggesting that $[\text{Au}_{25}(\text{SPG})_{18}]^-$ is a structural isomer of $[\text{Au}_{25}(\text{SR})_{18}]^-$ with an anisotropic Au core. The optical highest occupied molecular orbital (HOMO)-lowest unoccupied molecular orbital (LUMO) gap (HL^{opt}) of $[\text{Au}_{25}(\text{SPG})_{18}]^-$ (1.8 eV) was larger than HL^{opt} of $[\text{Au}_{25}(\text{SEtPh})_{18}]^-$ (1.3 eV), but comparable to HL^{opt} of $[\text{Au}_{23}(\text{ScHex})_{16}]^-$ (1.9 eV) (Figure 3a). Then, I theoretically searched for structural isomers using a model system $[\text{Au}_{25}(\text{SCH}_3)_{18}]^-$ (**A**). Initial structures were constructed based on the crystal structures of $[\text{Au}_{25}(\text{SEtPh})_{18}]^-$ [7, 8] and $[\text{Au}_{23}(\text{ScHex})_{16}]^-$ [10] (Figure 2). Structure optimization of **A** was conducted by density functional theory (DFT) calculation using the Gaussian 09 package with the level of TPSSH/Lan12DZ (Au) and 6-31G(d) (C, H, S). In addition to the well-known motif shown in Figure 2 (**A1**), I obtained an unprecedented motif (**A2**, Figure 4a) in which an anisotropic Au_{13} core is capped by two units of $\text{Au}_1(\text{SCH}_3)_2$, two units of

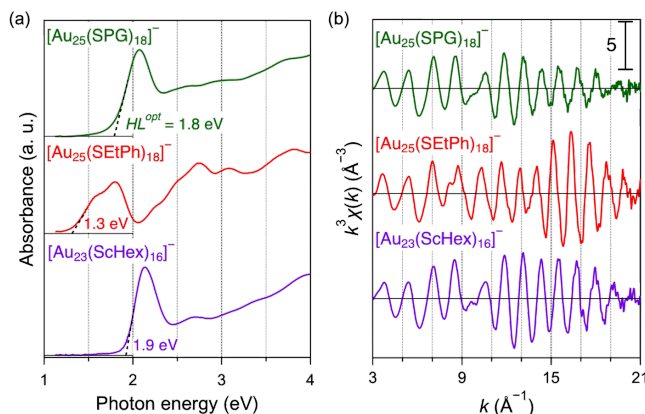


Figure 3 (a) Optical absorption spectra and (b) EXAFS oscillations of $[\text{Au}_{25}(\text{SPG})_{18}]^-$, $[\text{Au}_{25}(\text{SEtPh})_{18}]^-$, and $[\text{Au}_{23}(\text{ScHex})_{16}]^-$. The HL^{opt} of each cluster is shown in (a). EXAFS oscillations were measured at 10 K.

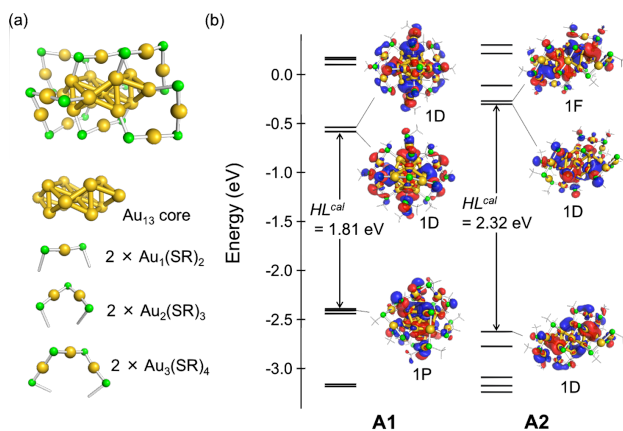


Figure 4 (a) Au-S framework of **A2**. Decomposed structure is shown below. (b) Energy diagrams around frontier orbitals of **A1** and **A2**. The Kohn-Sham orbitals and HL^{cal} of both structures are also shown.

$\text{Au}_2(\text{SCH}_3)_3$, and two units of $\text{Au}_3(\text{SCH}_3)_4$. I concluded that the structure **A2** is a plausible structural model for $[\text{Au}_{25}(\text{SPG})_{18}]^-$ because the simulations of optical absorption and EXAFS on **A2** reproduced the experimental results of $[\text{Au}_{25}(\text{SPG})_{18}]^-$. To gain an insight into the difference in the optical absorption between $[\text{Au}_{25}(\text{SPG})_{18}]^-$ and $[\text{Au}_{25}(\text{SEtPh})_{18}]^-$ (Figure 3a), the electronic structures of **A1** and **A2** are compared in Figure 4b. The Ih Au_{13} core of **A1** takes $(1\text{S})^2(1\text{P})^6$ electron configuration in which the degenerated 1P and 1D orbitals are the HOMOs and LUMOs, respectively. The calculated HOMO-LUMO gap (HL^{cal}) was 1.81 eV. On the other hand, the anisotropic Au_{13} core of **A2** takes an electron configuration of $(1\text{S})^2(1\text{P})^4(1\text{D})^2$ as in the case of $[\text{Au}_{23}(\text{ScHex})_{16}]^-$ [12] since the split 1D and 1F orbitals become the HOMO and LUMO, respectively. The HL^{cal} of **A2** was calculated to be 2.32 eV. The larger HL^{cal} of **A2** than **A1** (Figure 4b) is consistent with the larger HL^{opt} of $[\text{Au}_{25}(\text{SPG})_{18}]^-$ than $[\text{Au}_{25}(\text{SEtPh})_{18}]^-$ (Figure 3a). In summary, the formation of such anisotropic Au_{13} core having an electron configuration $(1\text{S})^2(1\text{P})^4(1\text{D})^2$ in $[\text{Au}_{25}(\text{SPG})_{18}]^-$ is probably caused by strong stress in ligand layer by interactions between PGS ligands having a secondary α -carbon, rigid amide group, and -COOH group.

3. Reduction resistance of $[\text{Au}_{25}(\text{SR})_{18}]^0$ protected by cyclohexanethiol

$\text{Au}_{25}(\text{ScHex})_{18}$ cluster was obtained as a minor byproduct of $[\text{Au}_{23}(\text{ScHex})_{16}]^-$ reported previously [10]. According to the results of single crystal X-ray diffraction (XRD) and optical absorption spectroscopy, $\text{Au}_{25}(\text{ScHex})_{18}$ had a neutral charge with an open electron configuration of $(1\text{S})^2(1\text{P})^5$. Conventionally, one-electron reduction of $[\text{Au}_{25}(\text{SEtPh})_{18}]^0$ through the reaction with 1 equiv of NaBH_4 was completed within 20 min to form $[\text{Au}_{25}(\text{SEtPh})_{18}]^-$ with a closed electron configuration of $(1\text{S})^2(1\text{P})^6$. However, $[\text{Au}_{25}(\text{ScHex})_{18}]^0$ did not undergo the reduction even after 60 min. This result suggests that $[\text{Au}_{25}(\text{ScHex})_{18}]^0$ prefers a neutral state with an open electron configuration of $(1\text{S})^2(1\text{P})^5$ rather than the anionic state with an 8 electrons closed shell.

To gain an insight into the origin of the reduction-resistant nature of $[\text{Au}_{25}(\text{ScHex})_{18}]^0$, the Au–Au bond lengths within the Au_{13} cores of $[\text{Au}_{25}(\text{SEtPh})_{18}]^-$, $[\text{Au}_{25}(\text{SEtPh})_{18}]^0$, and $[\text{Au}_{25}(\text{ScHex})_{18}]^0$ are compared in Figure 5. Broader distribution of the Au–Au bond lengths in $[\text{Au}_{25}(\text{SEtPh})_{18}]^0$ than in $[\text{Au}_{25}(\text{SEtPh})_{18}]^-$ demonstrates that the Au_{13} core of $[\text{Au}_{25}(\text{SEtPh})_{18}]^0$ is distorted by the Jahn-Teller effect while that of $[\text{Au}_{25}(\text{SEtPh})_{18}]^-$ is isotropic [13]. Thus, the fast reduction of $[\text{Au}_{25}(\text{SEtPh})_{18}]^0$ indicates that its distorted Au_{13} core is easily transformed into a higher symmetrical structure upon the reduction (Figure 6a). The Au_{13} core of $[\text{Au}_{25}(\text{ScHex})_{18}]^0$ is also distorted in a similar degree to that of $[\text{Au}_{25}(\text{SEtPh})_{18}]^0$ (Figure 5). Therefore, the retardation of the reduction of $[\text{Au}_{25}(\text{ScHex})_{18}]^0$ is ascribed to the difficulty in transforming the Au_{13} core into a highly symmetrical geometry upon the reduction (Figure 6b). The crystal structure analysis indicates that the ligand layer of $[\text{Au}_{25}(\text{ScHex})_{18}]^0$ has

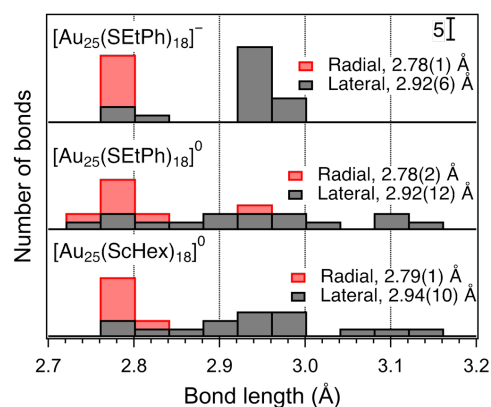


Figure 5. Histograms of Au–Au bond lengths within the Au_{13} cores of $[\text{Au}_{25}(\text{SEtPh})_{18}]^-$, $[\text{Au}_{25}(\text{SEtPh})_{18}]^0$, and $[\text{Au}_{25}(\text{ScHex})_{18}]^0$ [13]. The average bond lengths of radial and lateral Au–Au bonds are shown in the insets.

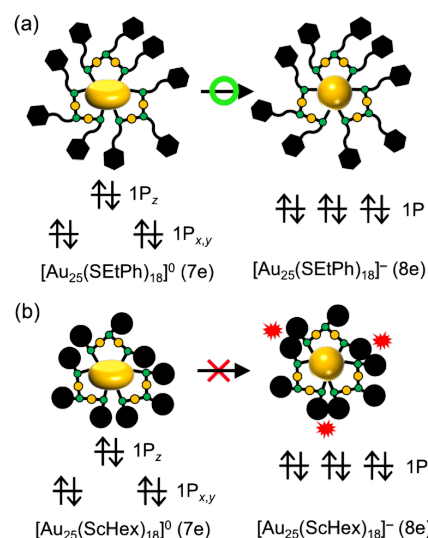


Figure 6 Schematic illustrations of the reduction of (a) $[\text{Au}_{25}(\text{SEtPh})_{18}]^0$ and (b) $[\text{Au}_{25}(\text{ScHex})_{18}]^0$ to the anionic species.

fewer degrees of freedom due to the close contacts between $\text{Au}_2(\text{ScHex})_3$ oligomers and restricts the structure of the Au_{13} . It is likely that the Au_{13} core of $[\text{Au}_{25}(\text{ScHex})_{18}]^0$ is forced to be deformed and cannot take a symmetrical structure because of bulky cHexS ligands.

4. Luminescence enhancement by introducing dendritic thiols

$[\text{Au}_{25}(\text{SEtPh})_{18-x}(\text{SDen})_x]^-$ and $[\text{Au}_{23}(\text{ScHex})_{16-x}(\text{SDen})_x]^-$ were prepared by ligand-exchange reaction of $[\text{Au}_{25}(\text{SEtPh})_{18}]^-$ and $[\text{Au}_{23}(\text{ScHex})_{16}]^-$ with DenSH. The average number of ligand exchange x_{ave} was estimated from their ESI mass spectra. I compared the PL of $[\text{Au}_{25}(\text{SEtPh})_{18-x}(\text{SDen})_x]^-$ and $[\text{Au}_{23}(\text{ScHex})_{16-x}(\text{SDen})_x]^-$ with unexchanged ones. Figure 7 plots the relative PL intensity of $[\text{Au}_{25}(\text{SEtPh})_{18-x}(\text{SDen})_x]^-$ and $[\text{Au}_{23}(\text{ScHex})_{16-x}(\text{SDen})_x]^-$ with different x_{ave} . Both exchanged products show stronger PL than unexchanged ones. Especially in the case of $[\text{Au}_{23}(\text{ScHex})_{16-x}(\text{SDen}^{\text{G}2})_x]^-$, its PL intensity was enhanced up to 15 times higher than that of $[\text{Au}_{23}(\text{ScHex})_{16}]^-$. The result is ascribed to that the non-radiative relaxation of the Au_{13} cores was suppressed by CH- π and/or π - π interactions between DenS ligands. Interestingly, $[\text{Au}_{25}(\text{SEtPh})_{18-x}(\text{SDen}^{\text{G}1})_x]^-$ shows stronger PL than $[\text{Au}_{25}(\text{SEtPh})_{18-x}(\text{SDen}^{\text{G}2})_x]^-$, whereas the trend is opposite in the case of $[\text{Au}_{23}(\text{ScHex})_{16-x}(\text{SDen})_x]^-$.

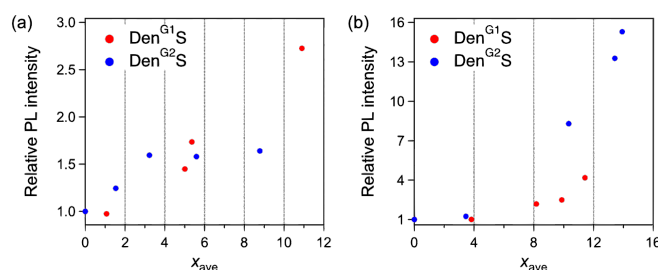


Figure 7 Plots of relative PL intensity of (a) $[\text{Au}_{25}(\text{SEtPh})_{18-x}(\text{SDen})_x]^-$ and (b) $[\text{Au}_{23}(\text{ScHex})_{16-x}(\text{SDen})_x]^-$ against x_{ave} . The data for $\text{Den}^{\text{G}1}\text{S}$ and $\text{Den}^{\text{G}2}\text{S}$ ligands are depicted as the red and blue dots, respectively.

5. Summary and prospects

In this study, I newly synthesized and characterized $\text{Au}_{25}(\text{SR})_{18}$ clusters protected by bulky thiolates with secondary α -carbon of PGS and cHexS. $[\text{Au}_{25}(\text{SPG})_{18}]^-$ had an anisotropic Au core in contrast to an Ih Au_{13} core in conventional $[\text{Au}_{25}(\text{SR})_{18}]^-$. Larger HOMO-LUMO gap of $[\text{Au}_{25}(\text{SPG})_{18}]^-$ than that of conventional $[\text{Au}_{25}(\text{SEtPh})_{18}]^-$ is ascribed to the reordering of the superatomic orbitals induced by the core deformation. The formation of an anisotropic core is probably induced by non-covalent interactions between PGS ligands. $[\text{Au}_{25}(\text{ScHex})_{18}]^0$ preferred neutral state with an open electron configuration of $(1\text{S})^2(1\text{P})^5$ and showed resistance to the reduction to close the electronic shell. The retardation of the reduction of $[\text{Au}_{25}(\text{ScHex})_{18}]^0$ is ascribed to that the bulky ligand layer of cHexS suppresses the relaxation of the Jahn-Teller distorted Au_{13} core to an isotropic geometry. In addition, I also introduced the Fréchet-type DenSH into $[\text{Au}_{25}(\text{SEtPh})_{18}]^-$ and $[\text{Au}_{23}(\text{ScHex})_{16}]^-$. Partially exchanged products showed the stronger PL than unexchanged ones. The PL enhancement is ascribed to that CH- π and/or π - π interactions between DenS ligands rigidify the Au cores and suppress non-radiative decay processes. These examples demonstrate that the optical properties and redox behavior of Au superatoms can be tuned by non-covalent interactions between ligands.

References

- [1] de Heer, W. A. *Rev. Mod. Phys.* **1993**, *65*, 611. [2] Omoda, T. *et al.*, *Small* in press. [3] Knoppe, S. *et al.*, *Acc. Chem. Res.* **2014**, *47*, 1318. [4] Narouz, M. R. *et al.*, *J. Am. Chem. Soc.* **2019**, *141*, 14997. [5] Ito, S. *et al.*, *J. Phys. Chem. Lett.* **2019**, *10*, 6892. [6] Zhang, L. *et al.*, *Langmuir* **2000**, *16*, 3813. [7] Heaven, M. W. *et al.*, *J. Am. Chem. Soc.* **2008**, *130*, 3754. [8] Zhu, M. *et al.*, *J. Am. Chem. Soc.* **2008**, *130*, 5883. [9] Walter, M. *et al.*, *Proc. Natl. Acad. Sci. USA* **2008**, *105*, 9157. [10] Das, A. *et al.*, *J. Am. Chem. Soc.* **2013**, *135*, 18264. [11] Negishi, Y. *et al.*, *J. Phys. Chem. B* **2006**, *110*, 12218. [12] Xiong, L. *et al.*, *J. Phys. Chem. C* **2018**, *122*, 14898. [13] Tofanelli, M. A. *et al.*, *Chem. Sci.* **2016**, *7*, 1882.